Geophys. J. Int. (1994) **117**, 733–748

Local 1-D interpretation of magnetotelluric B-polarization impedances

P. Weidelt[1] and P. Kaikkonen[2]

[1]*Institut für Geophysik und Meteorologie, Technische Universität Braunschweig, D-38106 Braunschweig, Germany*
[2]*Department of Geophysics, University of Oulu, SF-90570 Oulu, Finland*

Accepted 1993 November 25. Received 1993 November 25; in original form 1993 August 4

SUMMARY

It is shown that magnetotelluric impedances from the B-polarization (magnetic field in the strike direction of a 2-D resistivity structure) share a number of properties with 1-D impedances: all B-polarization impedances satisfy the same phase constraints as 1-D data, i.e. the impedance phase always lies between 0° and 90°. As a consequence the B-polarization impedances are minimum phase and thus allow conversions between apparent resistivity and phase. The constraints hold for an arbitrary 2-D topography of the air–earth interface. By examining the spectral function it is found that the B-polarization impedances for a number of models admit an exact 1-D interpretation. For two quarter-spaces this holds for all points and resistivity contrasts. The resulting 1-D model gives the correct resistivity down to a depth of half the distance to the interface. For the dyke model as the next complicated structure, 1-D interpretability requires that the host resistivity does not exceed the dyke resistivity by more than a factor of 60. B-polarization data of more complex structures investigated in this paper show either no, or only a marginal, violation of 1-D interpretability. A necessary condition constraining the frequency dependence of B-polarization and 1-D data in terms of their Mellin transform is derived in the final section.

Key words: B-polarization, magnetotellurics.

1 INTRODUCTION AND BASIC EQUATIONS

Whereas the analytical properties of the magnetotelluric transfer functions for 1-D structures are well explored (e.g. Weidelt 1972, 1986; Parker 1980; Yee & Paulson 1988a,b; Berdicevskij & Dmitriev 1992), very little reliable information is available for multidimensional structures. From an analytical point of view the B-polarization response (in the sequel abbreviated as 'B-response') is the simplest multidimensional response. In this polarization the magnetic field has only a component parallel to the strike direction and is constant at the air–earth interface. This simple boundary condition admits in some cases analytical solutions and is the reason that the surface impedance is simply the normalized tangential electric field rather than the ratio of two distorted local field components as in the E-polarization.

The present investigation was motivated by the question, whether there exist characteristic differences between 1-D and multidimensional responses, such that only an *approximate* 1-D interpretation could be found for an exact multidimensional response. A partial answer to this question is given by showing explicitly that some B-responses admit an exact 1-D interpretation. This has the practical consequence that a perfect 1-D fit will not necessarily imply a 1-D structure. This consequence, however, is not serious, since in general data in B- and E-polarization are available, and therefore the ambiguity of dimensionality is easily resolved.

There are two ways to test the one-dimensionality of a B-response at a given position: if the B-response is known in *analytical* form, a rigorous check is performed by testing the sign of the spectral function. If the B-response is given at a set of M discrete frequencies, 1-D consistency is checked by testing the signs of $2M$ determinants derived from the data (Weidelt 1986; Yee & Paulson 1988b). The latter grants a 1-D model for the given frequencies only, it may no longer exist for a denser frequency set.

The following model is considered: the half-space $z \geq 0$ with strike in x-direction has the resistivity distribution $\varrho(y, z)$, where for simplicity ϱ is bounded from below and

above, such that $0<\varrho<\infty$. Assuming a time factor $\exp(i\omega t)$, $\omega>0$ throughout, the three complex B-polarization field components B_x, E_y, E_z are related by

$$\varrho\partial_z B_x = \mu_0 E_y, \quad -\varrho\partial_y B_x = \mu_0 E_z,$$

$$\partial_y E_z - \partial_z E_y = -i\omega B_x,$$

where $\partial_y := \partial/\partial y$, etc. and $\mu_0 := 4\pi \times 10^{-7}$ Vs/(Am). The elimination of E_y and E_z yields, as the differential equation for B_x,

$$\nabla\cdot(\varrho\nabla B_x) = i\omega\mu_0 B_x, \tag{1}$$

which has to be solved subject to the inhomogeneous boundary condition

$$B_x(y, 0) = B_0, \tag{2}$$

where B_0 (being twice the inducing magnetic field) is the uniform field in the air half-space $z<0$.

The B-response is defined by Schmucker's transfer function (Schmucker 1970, p. 69)

$$c(y,\omega) := -\frac{E_y(y, z=0, \omega)}{i\omega B_0(\omega)} = -\frac{\varrho(y,0)\partial_z B_x(y,z,\omega)}{i\omega\mu_0 B_0(\omega)}\bigg|_{z=0}, \tag{3}$$

which is related to the surface impedance $Z = -\mu_0 E_y/B_x$ by

$$Z(y,\omega) = i\omega\mu_0 c(y,\omega).$$

In Appendix A it is shown by an eigenfunction expansion that $c(y,\omega)$ admits the spectral representation

$$c(y,\omega) = \int_{0-}^{\infty} \frac{a(y,\lambda)\,d\lambda}{\lambda + i\omega}. \tag{4}$$

The spectral function $a(y,\lambda)$ is connected with the values of c on the positive imaginary frequency axis by Stieltjes' relation (*cf.* Titchmarch 1967, p. 318)

$$a(y,\lambda) = -\frac{1}{\pi}\lim_{\epsilon\to 0^+} \mathcal{I}[c(y, i\lambda+\epsilon)], \tag{5}$$

where $\mathcal{I}$ denotes the imaginary part. On the other hand it is well known (Weidelt 1972; Parker 1980; Yee & Paulson 1988a) that the 1-D response can always be represented as

$$c(\omega) = a_0 + \int_{0-}^{\infty} \frac{a(\lambda)\,d\lambda}{\lambda + i\omega} \tag{6}$$

with

$$a(\lambda) = -\frac{1}{\pi}\lim_{\epsilon\to 0^+} \mathcal{I}[c(i\lambda+\epsilon)]$$

and

$$a_0 \geq 0, \quad a(\lambda)\geq 0. \tag{7}$$

Parker (1980) and Yee & Paulson (1988a) have shown that the conditions (7) are also sufficient for the existence of a 1-D model.

Three simple examples for the representation (6) are:

(1) uniform half-space with resistivity ϱ

$$c(\omega) = \sqrt{\frac{\varrho}{i\omega\mu_0}}, \qquad a_0 = 0, \qquad a(\lambda) = \frac{1}{\pi}\sqrt{\frac{\varrho}{\lambda\mu_0}};$$

(2) thin sheet with conductance τ at depth h

$$c(\omega) = h + \frac{1}{i\omega\mu_0\tau}, \qquad a_0 = h, \qquad a(\lambda) = \frac{1}{\mu_0\tau}\delta(\lambda);$$

(3) thin surface sheet with conductance τ and perfect conductor at depth h

$$c(\omega) = \frac{h}{1 + i\omega\mu_0\tau h}, \qquad a_0 = 0,$$

$$a(\lambda) = \frac{1}{\mu_0\tau}\delta(\lambda - \lambda_0), \qquad \lambda_0 = \frac{1}{\mu_0\tau h}.$$

This paper focuses on the determination of the spectral function $a(y,\lambda)$ in the representation (4) for simple analytical models. If, for a particular resistivity model, the spectral function $a(y,\lambda)$ at a particular site y is non-negative in the whole spectral range λ, then the B-response at site y admits a local 1-D interpretation. The additive constant a_0 in (6) is non-zero only for an insulating surface layer. In view of the assumption $\varrho<\infty$, it does not occur in the B-response presentation (4).

2 B-RESPONSE PHASE CONSTRAINTS

The B-response c shares with the 1-D response the property that it never leaves the fourth quadrant (or that the impedance Z always stays in the first quadrant). For a proof let

$$B_x/B_0 =: b\exp(i\psi), \tag{8}$$

where the phase ψ is considered as a continuous function (not modulo 2π). Then the insertion of eq. (8) into the differential equation (1) yields, after separating the real and imaginary parts

$$\nabla\cdot(\varrho\nabla b) = \rho b(\nabla\psi)^2, \tag{9}$$

$$\nabla\cdot(\varrho b^2\nabla\psi) = \omega\mu_0 b^2. \tag{10}$$

These equations show that neither b nor ψ can have a local maximum at an interior point of the half-space $z\geq 0$, because the necessary conditions for a local maximum of the function $f(y,z)$ ($= b$ or ψ), namely

$$\nabla f = 0, \quad \nabla^2 f < 0,$$

cannot be satisfied, since by virtue of

$$\nabla\cdot(\alpha\nabla f) = \nabla\alpha\cdot\nabla f + \alpha\nabla^2 f, \qquad \alpha>0$$

the left-hand sides of eqs (9) and (10) would be negative there, whereas the right-hand sides are non-negative. Therefore b and ψ attain their maxima at the boundary of the half-space $z\geq 0$. Assume for simplicity that for $y\to\pm\infty$ the resistivity $\varrho(y,z)$ tends to a layered structure $\varrho(z)$ (not necessarily the same at both sides). Then also $b = b(z)$ and $\psi = \psi(z)$ for $y\to\pm\infty$ and in view of $b\to 0$ for $z\to\infty$ we obtain from eqs (9) and (10):

$$b'(z) = -\frac{1}{\varrho(z)}\int_z^{\infty} \varrho(\zeta)b(\zeta)[\psi'(\zeta)]^2\,d\zeta < 0,$$

$$\psi'(z) = -\frac{\omega\mu_0}{\varrho(z)b^2(z)}\int_z^{\infty} b^2(\zeta)\,d\zeta < 0.$$

Therefore both b and ψ decrease at the left and right

boundary of the half-space $z \geq 0$, and on the lower boundary ($z \to \infty$) we have $b \to 0$ and $\psi \to -\infty$. Hence, the maxima of b and ψ are attained at $z = 0$, where $b = 1$ and $\psi = 0$.

In terms of b and ψ the B-response (3) reads

$$c(y) = -\frac{a(y, 0)}{i\omega\mu_0}(\partial_z b + i\partial_z \psi)|_{z=0}. \tag{11}$$

Since b and ψ have their maxima at $z = 0$, the derivatives in eq. (11) are non-positive. It is easily shown that they are in fact strictly negative (i.e. that the maxima at $z = 0$ are boundary maxima and not local maxima). The boundary condition (2) implies that $\partial_y \psi \equiv 0$ at $z = 0$. Assume that in addition $\partial_z \psi$ is vanishing at a point y of the interface $z = 0$. Then eq. (10) yields

$$\partial_{zz}^2 \psi|_{z=0} = \frac{\omega\mu_0}{\varrho(y, 0)} > 0,$$

which would lead to an increase of ψ when moving from the interface $z = 0$ into the conductor, contradicting the fact that ψ has its maximum at $z = 0$. Hence $\partial_z \psi < 0$ at $z = 0$. Similarly, by virtue of $\partial_y b \equiv 0$ at $z = 0$ the assumption $\partial_z b = 0$ at $z = 0$ would imply

$$\partial_{zz}^2 b|_{z=0} = (\partial_z \psi|_{z=0})^2 > 0,$$

which again leads to a contradicting increase of b when moving into the conductor. Hence also $\partial_z b < 0$ at $z = 0$. In conjunction with eq. (11) the two previous results imply that c lies strictly inside the fourth quadrant (or Z inside the first).

The phase constraints derived above for a plane air–earth interface ∂C hold in fact at each point P of an interface ∂C with an arbitrary 2-D topography, assuming only that ∂C is horizontal for $y \to \pm\infty$ and that the interface is sufficiently smooth at P, such that the curvature exists. Let $\hat{\mathbf{n}}$ be the unit normal vector at P pointing into the conductor C, and define the tangential unit vector by $\hat{\mathbf{t}} = \hat{\mathbf{n}} \times \hat{\mathbf{x}}$. Then again $B_x(P) = B_0$ and the maxima of b and ψ are attained at ∂C, where $b = 1$, $\psi = 0$, and

$$c(P) = -\frac{E_t(P)}{i\omega B_0} = -\frac{\varrho(P)\partial_n B_x}{i\omega\mu_0 B_0}\Big|_{\partial C}$$
$$= -\frac{\varrho(P)}{i\omega\mu_0}(\partial_n b + i\partial_n \psi)|_{\partial C}. \tag{12}$$

For $f = b$ or $f = \psi$ we have $\partial_t f(P) \equiv 0$ and

$$\nabla^2 f(P) = \partial_{nn}^2 f(P) + \kappa(P)\partial_n f(P),$$

where $\kappa(P)$ is the curvature of ∂C at P, being positive (negative) if the interface at P as seen from the air is convex (concave). By way of contradiction it is then again shown by means of eqs (11) and (10) that both $\partial_n \psi$ and $\partial_n b$ are strictly negative at P, thus recovering the phase constraints.

By a slight extension of the proof it can be shown that the B-response phase constraints even hold for arbitrary anisotropy (including dipping anisotropy). The proof relies on the fact that the resistivity tensor is positive definite (*cf.* also Protter & Weinberger 1969).

The tangential electric field component $E_t(P)$ is causally coupled to the inducing magnetic field $(1/2)B_0$. As a consequence the B-response (eq. 12) has no singularities in the half-plane $\mathcal{I}\omega \leq 0$, and real and imaginary part of c are related by a Hilbert transform pair (e.g. Nussenzveig 1972). The analyticity of the B-response in $\mathcal{I}\omega \leq 0$ is also demonstrated by the free-decay mode expansion (eq. A4) in Appendix A. It is easily seen that the phase constraints of the B-response imply that in addition to its analyticity c has no zeroes in $\mathcal{I}\omega \leq 0$, such that also $\log c$ is analytical there. For a proof let $\omega = \omega' - ip$. Since c is analytical for $p \geq 0$, $\mathcal{R}c$ (where $\mathcal{R}$ denotes the real part) satisfies the Laplace equation in the variables ω' and p. The boundary values of $\mathcal{R}c$ on the real axis satisfy the symmetry $\mathcal{R}c(-\omega') = \mathcal{R}c(\omega')$, are positive, and show the asymptotic behaviour $\mathcal{R}c = O(1/\sqrt{|\omega'|})$ for $|\omega'| \to \infty$. Therefore, the 2-D potential continuation integral

$$\mathcal{R}c(\omega' - ip) = \frac{p}{\pi}\int_{-\infty}^{+\infty} \frac{\mathcal{R}c(x)\,dx}{(x - \omega')^2 + p^2}, \qquad p > 0$$

exists and yields $\mathcal{R}c > 0$ for $p = -\mathcal{I}\omega > 0$. The positivity also follows from the minimum principle applied in the domain $\mathcal{I}\omega \leq 0$ to the non-constant harmonic function $\mathcal{R}c$ and its non-negative boundary values (e.g. Protter & Weinberger 1967).

The positivity of $\mathcal{R}c$ implies that c does not vanish for $\mathcal{I}\omega \leq 0$. Consequently there exist dispersion relations connecting $\log|c|$ (or the logarithm of the apparent resistivity $\varrho_a = \omega\mu_0|c|^2$) and the phase of c (or Z). Without fully establishing the analyticity of $\log c$ these relations have already been given by Fischer & Schnegg (1980). Let

$$c = \sqrt{\varrho_a/(\omega\mu_0)}\exp[i(\varphi - \pi/2)],$$

where $\varphi(\omega)$ is the impedance phase. Then

$$\log\frac{\varrho_a(\omega)}{\varrho_a(\infty)} = \frac{4}{\pi}\int_0^\infty \left[\frac{\pi}{4} - \varphi(x)\right]\frac{x\,dx}{x^2 - \omega^2},$$

$$\varphi(\omega) = \frac{\pi}{4} + \frac{\omega}{\pi}\int_0^\infty \log\frac{\varrho_a(x)}{\varrho_a(\infty)}\frac{dx}{x^2 - \omega^2}$$

where $\varrho_a(\infty) = \varrho(P)$.

3 THE QUARTER-SPACE MODEL

3.1 The spectral function $a(y, \lambda)$

The simplest model in B-polarization are two quarter-spaces with $\varrho = \varrho_1$ in $y < 0$ and $\varrho = \varrho_2$ in $y > 0$. In the vertical direction the quarter-spaces extend to infinity. The solution was first given by d'Erceville & Kunetz (1962):

$$c(y, \omega) = \frac{1}{k_1} + \frac{2}{\pi}(\varrho_1 - \varrho_2)\int_0^\infty \frac{s^2\exp(-\alpha_1|y|)\,ds}{\alpha_1^2\alpha_2(\alpha_1\varrho_1 + \alpha_2\varrho_2)}, \qquad y < 0 \tag{13}$$

$$c(y, \omega) = \frac{1}{k_2} - \frac{2}{\pi}(\varrho_1 - \varrho_2)\int_0^\infty \frac{s^2\exp(-\alpha_2 y)\,ds}{\alpha_1\alpha_2^2(\alpha_1\varrho_1 + \alpha_2\varrho_2)}, \qquad y > 0 \tag{14}$$

with

$$k_m^2 := i\omega\mu_0/\varrho_m, \qquad \alpha_m^2 := s^2 + k_m^2, \qquad m = 1, 2.$$

The spectral function $a(y, \lambda)$ is most easily estimated after, according to eq. (5), putting $\omega = i\lambda$, rotating the contour in the s-plane counter-clockwise by an angle $\pi/2$, assuring that

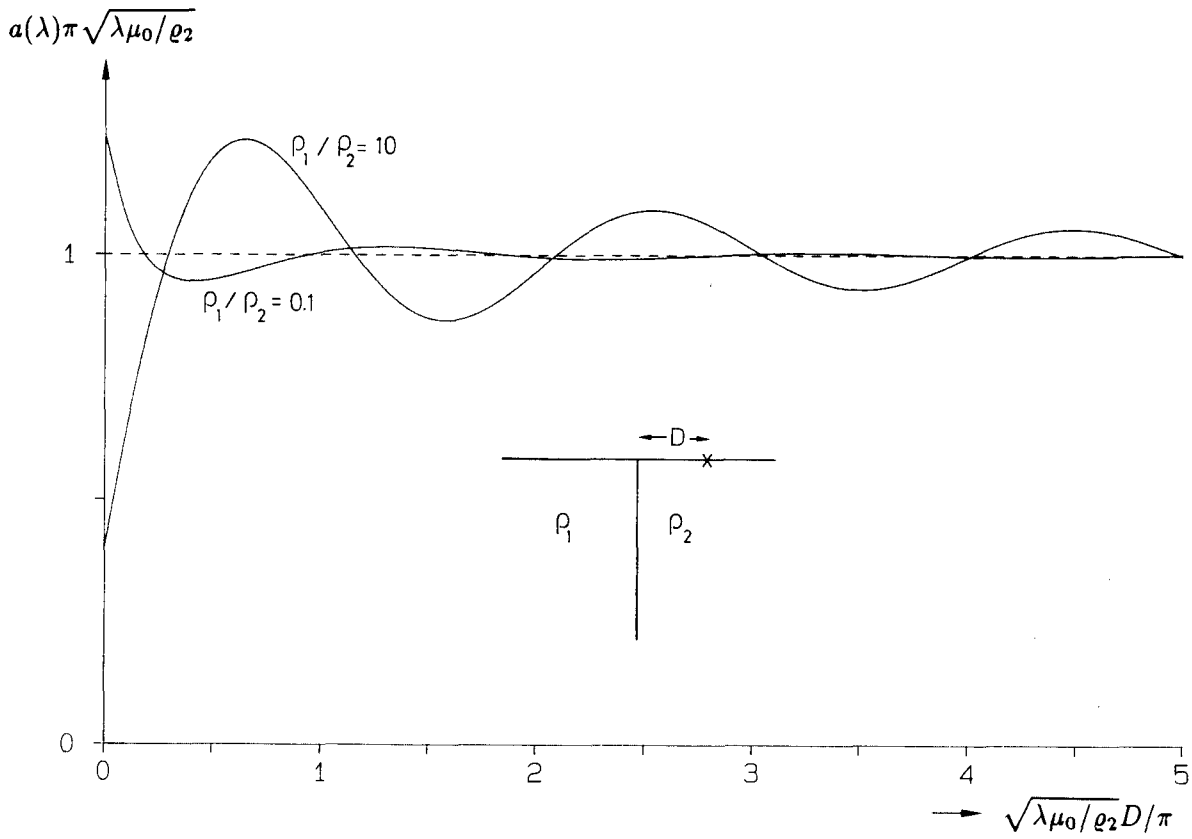

Figure 1. The spectral function at $y = D$ above the quarter-space ϱ_2. The ordinate is $\pi\mu_2 a(\lambda)$, which tends to 1 for $\lambda \to \infty$. The oscillations of period 2 are well developed only over the conductive quarter-space ($\varrho_1/\varrho_2 = 10$).

no singularity is crossed, and introducing

$$t := -is, \quad u_m := \sqrt{\lambda\mu_0/\varrho_m}, \quad \beta_m := \sqrt{t^2 + \mu_m^2}. \tag{15}$$

Then $\alpha_m = i\beta_m$, and we obtain for $y > 0$ (say)

$$\pi a(y, \lambda) = \frac{1}{\mu_2} - \frac{2}{\pi}(\varrho_1 - \varrho_2)\int_0^\infty \frac{t^2 \cos(\beta_2 y)\, dt}{\beta_1\beta_2^2(\beta_1\varrho_1 + \beta_2\varrho_2)}. \tag{16}$$

Now

$$\frac{t^2 \cos(\beta_2 y)}{\beta_1(\beta_1\varrho_1 + \beta_2\varrho_2)} \le \frac{t^2}{\beta_1(\beta_1\varrho_1 + \beta_2\varrho_2)} \le \frac{1}{\varrho_1 + \varrho_2},$$

and therefore

$$\pi a(y, \lambda) \ge \frac{1}{\mu_2} - \frac{|\varrho_1 - \varrho_2|}{\varrho_1 + \varrho_2}\frac{2}{\pi}\int_0^\infty \frac{dt}{\beta_2^2} = \frac{1}{\mu_2}\left(1 - \frac{|\varrho_1 - \varrho_2|}{\varrho_1 + \varrho_2}\right) > 0.$$

For $y < 0$ interchange the subscripts 1 and 2. Consequently, B-responses from quarter-spaces admit a 1-D interpretation for all resistivity contrasts and points of observation. Fig. 1 represents the spectral function over a poor and a good conductor. Only the latter leads to significant departures from the local uniform half-space.

3.2 1-D reconstruction from the spectral function

There are different methods for the reconstruction of a 1-D resistivity distribution $\varrho(z)$ below point y from its spectral function $a(y, \lambda)$. Two of them, namely those of Gopinath & Sondhi and Gel'fand & Levitan are briefly summarized. For ease of notation the explicit dependence on y is not shown in the sequel.

First, we deduce from the high frequency behaviour of $c(\omega)$ or the large decay constant behaviour of $a(\lambda)$ the surface resistivity

$$\varrho(0) =: \varrho_0 = \lim_{\omega\to\infty} i\omega\mu_0 c^2(\omega) = \lim_{\lambda\to\infty} \lambda\mu_0\pi^2 a^2(\lambda).$$

Then λ and $\varrho(z)$ serve to define a wavenumber μ and a depth coordinate x through

$$\mu := \sqrt{\lambda\mu_0/\varrho_0}, \qquad x := \int_0^x \sqrt{\varrho_0/\varrho(t)}\, dt. \tag{17}$$

The reconstruction of $\varrho(z)$ is performed in two steps.

Step 1: Fourier transform of $\tilde{a}(\mu) := a(\lambda)$ to construct the kernel $B(x)$

$$B(x) = \begin{cases} 0, & x < 0 \\ \dfrac{1}{\pi}\displaystyle\int_0^\infty [1 - \pi\mu\tilde{a}(\mu)]\cos(\mu x)\, d\mu, & x \ge 0. \end{cases} \tag{18}$$

Step 2: solution of a linear integral equation with the kernel $B(x)$.

(i) Gopinath & Sondhi (Whittall & Oldenburg 1986)

$$F(x, u) = 1 + \int_{-x}^{+x} F(x, t)B(|u - t|)\, dt, \qquad |u| \le x, \tag{19}$$

$$\tilde{\varrho}(x) = \varrho_0 / F^4(x, x). \tag{20}$$

(ii) Gel'fand & Levitan (Weidelt 1972)

$$A(x, u) = B(x + u) + \int_{-x}^{+x} A(x, t)[B(u + t) - B(u - t)]\, dt, \qquad |u| \le x, \tag{21}$$

$$\tilde{\varrho}(x) = \varrho_0 \Big/ \left[1 + \int_{-x}^{+x} A(x, t)\, dt\right]^4, \tag{22}$$

$$z(x) = \left[x + \int_{-x}^{+x} A(x, t) t\, dt\right] \Big/ \left[1 + \int_{-x}^{+x} A(x, t)\, dt\right]. \tag{23}$$

The linear integral equations (19) or (21) are solved with x as a fixed positive parameter. With the solutions F or A the resistivity $\tilde{\varrho}(x)[=\varrho(z)]$ with respect to the distorted depth coordinate x is obtained using eqs (20) and (22). The true depth z then follows from

$$dz = \sqrt{\tilde{\varrho}(x)/\varrho_0}\, dx,$$

or in case of the Gel'fand–Levitan method also directly from eq. (23). If the 1-D constraints are violated by negative values of $\tilde{a}(\mu)$, then

$$F(x, x) \quad \text{or} \quad 1 + \int_{-x}^{+x} A(x, t)\, dt$$

will also become negative somewhere.

Now the reconstruction algorithms are applied to the quarter-space data. Let $y = D > 0$. Then according to eqs (15) and (17) $\mu = \mu_2$. For a determination of $B(x)$ the spectral function (16) is inserted into eq. (18). In eq. (16) the variable t is replaced by ξ on using

$$\beta_2 y = \beta_2 D = \mu\xi, \quad \text{i.e.} \quad t = \mu\sqrt{\xi^2 - D^2}/D.$$

After changing the order of integration the μ-integration simplifies to

$$\frac{2}{\pi}\int_0^{\infty} \cos(\mu\xi)\cos(\mu x)\, d\mu = \delta(x - \xi) + \delta(x + \xi).$$

Since the range of integration starts at $\xi = D$, the kernel $B(x)$ is given by

$$B(x) = \begin{cases} 0, & 0 \le x \le D \\ \dfrac{(1 - r)D\sqrt{x^2 - D^2}}{\pi x\sqrt{x^2 + (r - 1)D^2}\left[rx + \sqrt{x^2 + (r - 1)D^2}\right]}, & x \ge D \end{cases}$$

with $r := \varrho_2/\varrho_1$. The result $B(x) = 0$ for $0 \le x \le D$ implies that for $x \le D/2$ the integral equations (19) or (21) are solved by $F = 1$ or $A = 0$. Therefore

$$\varrho(z) = \varrho_m \quad \text{for} \quad 0 \le z \le D/2,$$

i.e. down to a depth of half the distance to the interface the B-response gives the true resistivity. The numerical solution of eq. (19) or eq. (21) using $B(x)$ given above then shows that below this depth the resistivity even *increases* on the resistive side and *decreases* on the conductive side (*cf.* Fig. 2). On putting $s = k_2 \tan\epsilon$ we derive from eq. (14) for $y > 0$ the limit

$$\lim_{z\to\infty} \sqrt{\varrho(z)/\varrho_2} = \lim_{\omega\to 0} k_2 c(y, \omega)$$

$$= \sqrt{\frac{r}{1 + r}} + \frac{2r}{\pi}\int_0^{\pi/2} \frac{\sin^2\epsilon\, d\epsilon}{(r + \sin^2\epsilon)\sqrt{\sin^2\epsilon + r\cos^2\epsilon}}.$$

This limit holds for $y \ll z$. For $y \to 0^+$, i.e. to the right of the vertical interface, this asymptotic value is already reached for $z = 0$. If the quarter-space $y < 0$ is highly resistive ($r \to 0$), the asymptotic resistivity in $y > 0$ tends to zero. If, however, the quarter-space $y < 0$ approaches a perfect conductor ($r \to \infty$), it does not affect the asymptotic

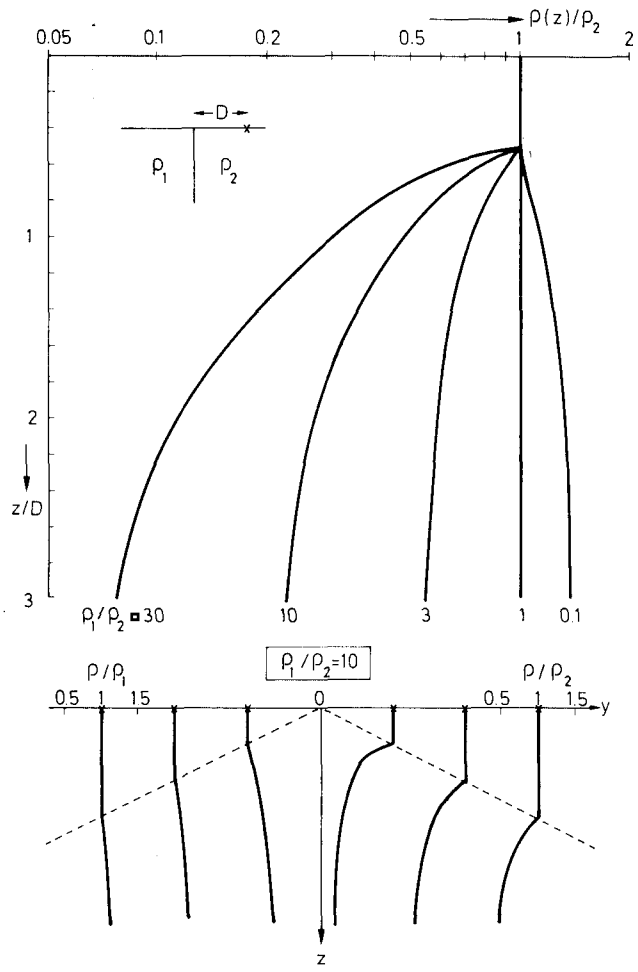

Figure 2. The B-response of two quarter-spaces in a 1-D interpretation. Top: the normalized resistivity profiles below the point $y = D > 0$ for different resistivity ratios ϱ_1/ϱ_2. The true resistivity is obtained in the depth range $0 \le z \le D/2$. Below that depth the resistivity increases (decreases) over the resistive (conductive) quarter-space. The dependence on the resistivity in the adjacent quarter-space is much more pronounced on the conductive side. Bottom: resistivity profiles at both sides of the discontinuity for $\varrho_1/\varrho_2 = 10$ and different interface distances D, which determine the vertical scale length.

resistivity, $\varrho(\infty) = \varrho_2$ and therefore $\varrho(z) \equiv \varrho_2$. The greatest effect is obtained for $r \simeq 9.05$, where $\varrho(\infty)/\varrho_2 \simeq 1.5835$. The apparent enhancement of the resistivity contrast (starting at increasing depth when leaving the discontinuity) results from $E_y(0^+, z)/E_y(0^-, z) = r$, implying in particular $\varrho_a(0^+)/\varrho_a(0^-) = r^2$. Therefore the ratio between the asymptotic resistivities in $y > 0$ and $y < 0$ is r^2 rather than the true value r.

In the quarter-space model the 1-D interpretation gives the true resistivity down to a depth of half the distance to the interface. In Appendix B this result is generalized by showing that in a segmented half-space the 1-D resistivity is correct down to half the distance to the closest interface.

4 THE DYKE MODEL

The experience obtained from the simple quarter-space model cannot be generalized to more complicated structures. Already the dyke model (*cf.* Fig. 3) as the next complicated structure reveals that an unconditional 1-D interpretation of the B-response is possible only for resistive dykes. For conductive dykes the 1-D interpretation breaks down first for points of observation in the centre of the dyke, if this is more than 60 times better conducting than the host.

Let us denote the resistivities of the host and dyke by ϱ_1 and ϱ_2, respectively, and let again $r = \varrho_2/\varrho_1$, where $r < 1$ for a conductive dyke. Moreover, let k_m, α_m, β_m, and μ_m, $m = 1,2$ have the same meaning as in Section 3.1. If the dyke extends from $y = -D$ to $y = +D$, then B-response and spectral function in the centre of the dyke ($y = 0$) are given by

$$c(0, \omega) = \frac{1}{k_2} - \frac{2(1-r)}{\pi} \times \int_0^\infty \frac{s^2\, ds}{\alpha_1 \alpha_2^2 [\alpha_1 \cosh(\alpha_2 D) + \alpha_2 r \sinh(\alpha_2 D)]}, \quad (24)$$

$$\pi a(0, \lambda) = \frac{1}{\mu_2} - \frac{2(1-r)}{\pi} \times \int_0^\infty \frac{t^2 \cos(\beta_2 D)\, dt}{\beta_2^2 [\beta_1^2 \cos^2(\beta_2 D) + \beta_2^2 r^2 \sin^2(\beta_2 D)]}. \quad (25)$$

The B-response can be obtained from the method described in Appendix B. Alternatively it can be deduced from the solutions given by Rankin (1962) or Wait & Spies (1974). As in Section 3.1 the spectral function is again easily calculated by rotating the line of integration in the s-plane by $\pi/2$. Fig. 3 shows the normalized spectral function $\pi\mu_2 a(\lambda)$ as a function of the non-dimensional quantity $\mu_2 D/\pi \sim \sqrt{\lambda}$ for various resistivity ratios ϱ_1/ϱ_2. The spectral function remains positive for $\varrho_1/\varrho_2 < 60$, but for greater contrasts it attains negative values near $\mu_2 D/\pi = 1.5$, which inhibits a 1-D interpretation at the central point. Non-central points on the dyke show the same behaviour at greater contrasts.

The dyke spectral function shows distinct peaks at

$$\mu_2 D/\pi \simeq n + 1/2, \qquad n = 0, 1, 2, \ldots$$

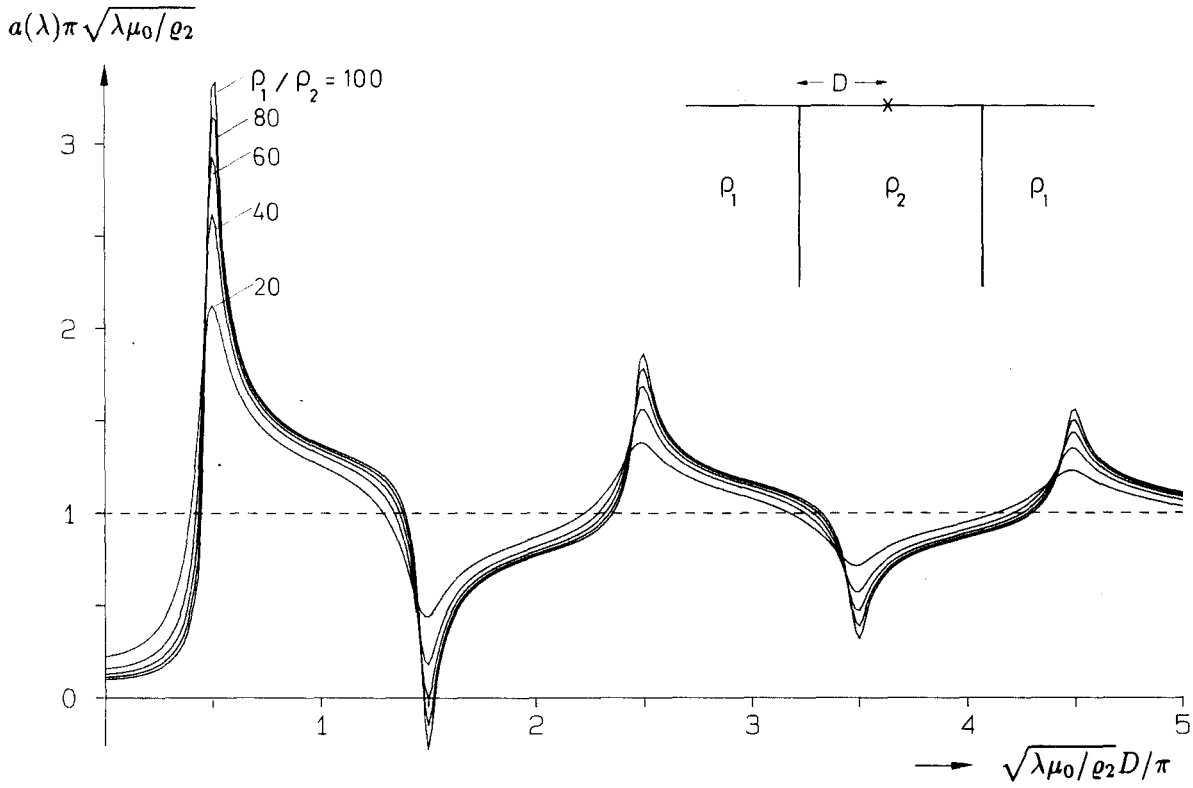

Figure 3. Normalized spectral function for a site at the centre of a conducting dyke of width $2/D$ for different ratios ϱ_1/ϱ_2. The spectral functions have a negative spike for $\varrho_1/\varrho_2 > 60$, which destroys the 1-D character of the corresponding data (but should be hardly visible in real data). Over a resistive dyke the spectral function is always positive.

The origin of these peaks is best explained by appealing to the free-decay mode expansion of the B-response as outlined in Appendix A. Separating the z-dependence by assuming a variation $\sim\sin(vz)$ (*cf.* eq. A7), the relevant eigenvalue equation is

$$\varphi''(y) + (\mu_m^2 - v^2)\varphi(y) = 0,$$

with $m = 1$ for $|y| > D$ and $m = 2$ for $|y| < D$, subject to the continuity of φ and $\varrho\varphi'$ at $y = \pm D$. The eigenvalue λ is buried in μ_m, where $\mu_1 = \sqrt{r}\mu_2$. Since the expansion coefficients (A5) are proportional to the horizontal average of the decay modes, only the symmetrical modes contribute. It is easily seen that the eigenvalue problem admits two types of free-decay modes:

(1) $v \le \mu_1 \le \mu_2$—oscillating fields both in the resistive host (long-wavelength $2\pi/\sqrt{\mu_1^2 - v^2}$) and in the conductive dyke (short-wavelength $2\pi/\sqrt{\mu_2^2 - v^2}$);

(2) $\mu_1 \le v \le \mu_2$—exponentially decaying fields in the resistive host (scale length $1/\sqrt{v^2 - \mu_1^2}$) and oscillations confined to the conductive dyke (wavelength as above).

In the first case there exists for a given vertical wavenumber v a continuum of horizontal wavenumbers u_1 and u_2, $0 \le u_1 \le u_2 < \infty$, satisfying

$$\lambda = \varrho_1(u_1^2 + v^2)/\mu_0 = \varrho_2(u_2^2 + v^2)/\mu_0,$$

whereas in the second case a given v is associated with a finite number of discrete horizontal wavenumbers $\sqrt{\mu_2^2 - v^2}$, defined by the eigenvalue equation

$$r\tan(\sqrt{\mu_2^2 - v^2}D) = \sqrt{\frac{v^2 - \mu_1^2}{\mu_2^2 - v^2}}.$$

This equation associates a given v with a number of branches, identified by the quantum number n, $n = 0, 1, 2, \ldots$ Branch n is excited if v exceeds the threshold v_n, where

$$v_n = \mu_1, \quad \sqrt{\mu_2^2 - v_n^2}D = n\pi,$$

i.e.

$$v_n = \frac{n\pi}{D}\sqrt{\frac{r}{1-r}}, \quad \mu_2 = \frac{n\pi}{D\sqrt{1-r}}.$$

For $\varrho_1/\varrho_2 = 20$ Fig. 4 shows the normalized eigenvalue $\mu_2 D/\pi$ as a function of Dv. For a given v, discrete spectral lines (branches) occur for $v < \mu_2 < v/\sqrt{r}$, whereas the spectrum is continuous beyond. The crosses mark the cut-off values v_n and corresponding eigenvalues μ_2. As an example, the discrete lines $n = 0 \to 4$ are excited for $Dv = 3$. The associated eigenfunctions are displayed in Fig. 5. In order that the B-response expansion coefficient as a function of y has the same sign as the corresponding eigenfunction, we have chosen in view of eq. (A5) that polarity, which yields a positive average. The quantum number n counts the negative half-waves. The eigenvalue λ (or μ_2) is a measure of the total variability of the decay mode. For fixed vertical variability (fixed v) the horizontal variability increases with μ_2. This is exemplified in Fig. 5 with $\mu_2 D/\pi$ given to the left. If μ_2 exceeds $v/\sqrt{r}$ (corresponding to $\mu_2 D/\pi \simeq 4.27$), the eigenfunctions become oscillatory also in $|y| > D$.

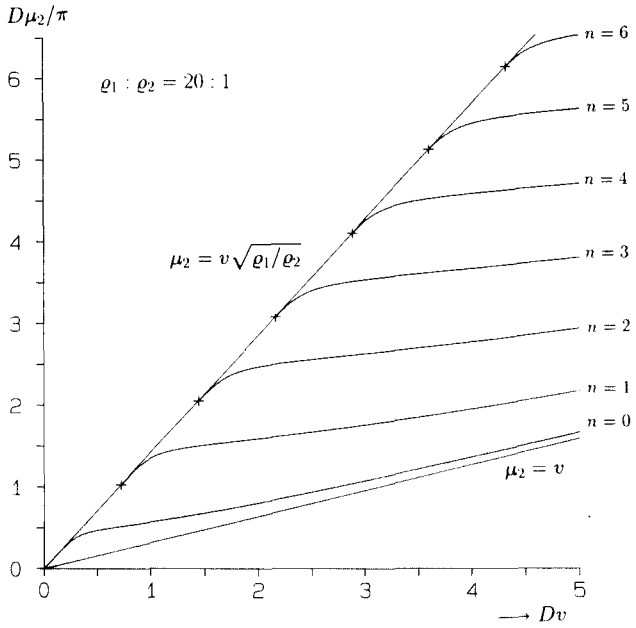

Figure 4. Structure of the conducting dyke free-decay spectrum for $\varrho_1/\varrho_2 = 20$. The eigenvalue $\mu_2^2 = u_2^2 + v^2$ as the sum of the squared wavenumbers v (in the vertical direction) and u_2 (in the horizontal direction) is a measure of the variability of the corresponding eigenfunction in the dyke. For a given v no mode can be excited for $\mu_2 < v$, since both in the conductor and resistor the field would vary exponentially in the horizontal direction and would not admit to satisfy the boundary conditions at the interface and at infinity. In the range $v < \mu_2 < v\sqrt{\varrho_1/\varrho_2}$, however, a finite number of discrete lines (labelled by the number n of negative half-waves in the dyke) can be excited. In the resistive host the field still decays exponentially in the horizontal direction. If μ_2 exceeds $v\sqrt{\varrho_1/\varrho_2}$, the eigenfunction shows a horizontal oscillation also in the resistor, which then allows a continuous spectrum.

The discrete symmetrical modes trapped in the conducting dyke are responsible for the peaks occurring in the spectral function (*cf.* Fig. 3). With the polarity explained above they have the asymptotic form ($y = 0$ in the centre of the dyke)

$$(-1)^n \cos(n\pi y/D), \quad v \to \mu_1^+$$

and

$$(-1)^n \cos[(n + \tfrac{1}{2})\pi y/D], \quad v \to \mu_2^-.$$

With reference to eq. (A5), at $y = 0$ the branches $n = 1, 3, 5, \ldots$ contribute to the downward peaks and $n = 0, 2, 4, \ldots$ to the upward peaks. It is seen in Fig. 4 that $\mu_2 D/\pi$ is close to $n + 1/2$ for a wide range of vertical wavenumbers. The branch $n = 1$ leads to the most pronounced downward peak and is responsible for the negative values of $a(\lambda)$ for $\varrho_1/\varrho_2 > 60$. (It is seen from Figs 3 and 4 that for $\varrho_1/\varrho_2 = 20$ the vertical wavenumber $Dv \simeq 1.5$ yields the dominant contribution.) The following downward peaks ($n = 3, 5, \ldots$) are weaker (*cf.* Fig. 3), because the mode average decreases with n (*cf.* eq. (A5) and Fig. 5).

An idea of the qualitative behaviour of the spectral function may also be formed by considering the unphysical

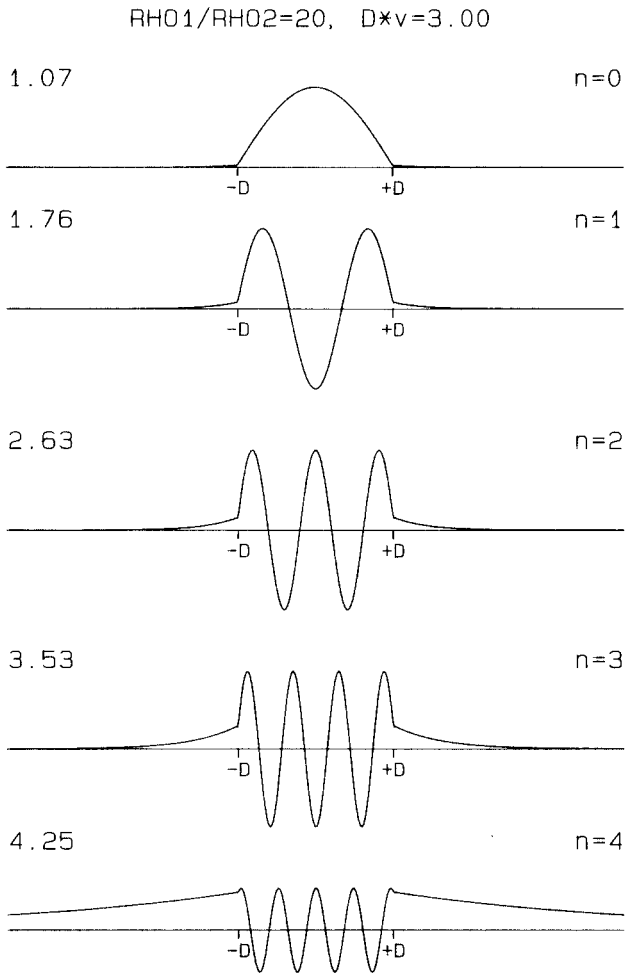

Figure 5. Horizontal variation of the discrete free-decay modes excited in the model of Fig. 4 for $Dv = 3$. On the left the normalized eigenvalues $\mu_2 D/\pi$ are given.

extreme contrast case $\varrho_1 \to \infty$. Then eq. (24) reduces to

$$c(0, \omega) = \frac{1}{k_2} - \frac{2}{\pi}\int_0^\infty \frac{ds}{\alpha_2^2 \cosh(\alpha_2 D)},$$

from which—using the recipe (5)—the spectral function follows with the calculus of residues,

$$\pi a(0, \lambda) = \frac{2}{\pi}\sum_{j=0}^{n} \frac{(-1)^j}{(j+1/2)\sqrt{\mu_2^2 - (j+1/2)^2\pi^2/D^2}},$$

$$n := [\mu_2 D/\pi - 1/2],$$

where $[x]$ denotes the greatest integer $\leq x$. The spectrum shows a sequence of peaks with sign $(-1)^n$ whenever $\mu_2 D/\pi$ just exceeds $n + 1/2$.

From the simple models considered so far one may tend to anticipate that the failure of 1-D interpretability of the B-response is restricted to high contrasts. However, remaining in the class of resistivity models $\varrho(y, z) = \varrho(y)$, $z \geq 0$ we were able to construct a special low-contrast model with a contrast lower than 4, which was not 1-D at all points.

5 QUARTER-SPACES WITH INSULATING OR CONDUCTIVE SUBSTRATUM

The simplest modification of the quarter-space model considered in Section 3, where the quarter-spaces extend in the vertical direction to infinity, is the addition of a horizontal interface at $z = H$, below which the resistivity is either zero or infinite. Also this model has been first treated by d'Erceville & Kunetz (1962). For $y > 0$ (say) the B-responses are

$$c(y, \omega) = \frac{1}{k_2}\tanh(k_2 H) - \frac{2}{H}(\varrho_1 - \varrho_2)\sum_{n=0}^{\infty} \frac{s_n^2 \exp(-\alpha_{2n} y)}{\alpha_{1n}\alpha_{2n}^2(\alpha_{1n}\varrho_1 + \alpha_{2n}\varrho_2)} \quad (26)$$

with $s_n = (n + \frac{1}{2})\pi/H$ for a perfectly conducting substratum and

$$c(y, \omega) = \frac{1}{k_2}\coth(k_2 H - \frac{2}{H}(\varrho_1 - \varrho_2)\sum_{n=1}^{\infty} \frac{s_n^2 \exp(-\alpha_{2n} y)}{\alpha_{1n}\alpha_{2n}^2(\alpha_{1n}\varrho_1 + \alpha_{2n}\varrho_2)} \quad (27)$$

with $s_n = n\pi/H$ for a perfectly insulating basement. Used are the abbreviations

$$\alpha_{mn}^2 := s_n^2 + k_m^2, \quad k_m^2 := i\omega\mu_0/\varrho_m.$$

For $y < 0$ the subscripts 1 and 2 are interchanged and y is replaced by $|y|$. For $H \to \infty$ eqs (26) and (27) merge into eq. (14) by the substitutions $s_n \to s$, $\pi/H \to ds$.

A modification of the B-response (eq. 26) for the perfectly conducting substratum as proposed by Groom & Bailey (1989) is not justified. The solution of d'Erceville & Kunetz satisfies the differential equation (1) (including the continuity of tangential electric and magnetic fields at the vertical interface), $B_x = B_0$ at $z = 0$, and $E_y = 0$ at $z = H$, and therefore constitutes—by an easily established uniqueness theorem—the only solution of the problem. (It appears that the Groom–Bailey solution violates the boundary condition $E_y = 0$ at $z = H$.)

According to the recipe (5) the spectral functions of eqs (26) and (27) are constructed by considering the B-response at positive imaginary frequencies. Here both the normal part and the anomalous part (the sum) have simple poles at $\alpha_{2n}^2 = 0$, i.e. at $\omega = i\lambda_n = is_n^2\varrho_2/\mu_0$. In view of the Mittag–Leffler expansions (using the pertaining definition of s_n)

$$\frac{1}{k_2}\tanh(k_2 H) = \frac{2}{H}\sum_{n=0}^{\infty}\frac{1}{\alpha_{2n}^2},$$

$$\frac{1}{k_2}\coth(k_2 H) = \frac{1}{k_2^2 H} + \frac{2}{H}\sum_{n=1}^{\infty}\frac{1}{\alpha_{2n}^2},$$

the pole contributions cancel (except at the origin) and do not require further consideration. In addition to a pole, each term in the sums has a branch point at $\lambda = s_n^2\varrho_m/\mu_0$, $m = 1,2$. Let again

$$\mu_m^2 := \lambda\mu_0/\varrho_m \quad \text{and} \quad \bar{\alpha}_{mn}^2 := -\alpha_{mn}^2 = \mu_m^2 - s_n^2.$$

Then for $y = D > 0$ and $\varrho_2 < \varrho_1$

$$\mathcal{F}\left[\frac{(\varrho_1 - \varrho_2)s_n^2 \exp(-\alpha_{2n}D)}{\alpha_{1n}\alpha_{2n}^2(\alpha_{1n}\varrho_1 + \alpha_{2n}\varrho_2)}\right] \rightarrow \begin{cases} D/\bar{\alpha}_{2n} & \text{for } \lambda \rightarrow s_n^2\varrho_2/\mu_0 + 0 \\ +\cos(\bar{\alpha}_{2n}D)/(\alpha_{1n}\bar{\alpha}_{2n}) & \text{for } \lambda \rightarrow s_n^2\varrho_1/\mu_0 - 0, \\ -\sin(\bar{\alpha}_{2n}D)/(\bar{\alpha}_{1n}\bar{\alpha}_{2n}) & \text{for } \lambda \rightarrow s_n^2\varrho_1/\mu_0 + 0 \end{cases}$$

whereas for $\varrho_2 > \varrho_1$

$$\mathcal{F}_3\left[\frac{(\varrho_1 - \varrho_2)s_n^2 \exp(-\alpha_{2n}D)}{\alpha_{1n}\alpha_{2n}^2(\alpha_{1n}\varrho_1 + \alpha_{2n}\varrho_2)}\right] \rightarrow \begin{cases} \exp(-\alpha_{2n}D)/(\bar{\alpha}_{1n}\alpha_{2n}) & \text{for } \lambda \rightarrow s_n^2\varrho_1/\mu_0 + 0 \\ (\varrho_2/\varrho_2)/(\bar{\alpha}_{1n}\alpha_{2n}) & \text{for } \lambda \rightarrow s_n^2\varrho_2/\mu_0 - 0. \\ D/\bar{\alpha}_{2n} & \text{for } \lambda \rightarrow s_n^2\varrho_2/\mu_0 + 0 \end{cases}$$

In both cases the spectral function $a(\lambda)$ is structured by a periodic sequence of positive peaks at $\mu_2 = s_n$, where $a(\lambda)$ varies for $\mu_2 \rightarrow s_n^+$ as $1/\bar{\alpha}_{2n} = 1/\sqrt{\mu_2^2 - s_n^2}$. In addition, there occurs a periodic sequence of peaks at $\mu_1 = s_n$. In the conductive case ($\varrho_2 < \varrho_1$) these peaks are negative, whenever the angle $\bar{\alpha}_{2n}D = s_nD\sqrt{\varrho_1/\varrho_2 - 1}$ (modulo 2π) is outside the fourth quadrant. Therefore, both for an insulating and a conducting substratum the B-response on the conductive side violates the 1-D constraints for all resistivity ratios and all interface depths $H < \infty$. In the resistive case ($\varrho_2 > \varrho_1$) the peaks are positive and their amplitudes decay as

$$\exp(-\alpha_{2n}D) = \exp(-s_nD\sqrt{1 - \varrho_1/\varrho_2}).$$

Although not obvious, also in this case the substratum spoils the 1-D character of the B-response, because for $\lambda \rightarrow \infty$ the spectral function drops down to (small) negative values between adjacent positive peaks at $\mu_2 = s_n$. However, the spectral function averaged in μ_2 over the period π/H becomes a smooth positive function and approaches for $H/D \gg 1$ the limits shown in Fig. 1.

For a conductive substratum and $H/D = 10$ Figs 6 and 7 show the normalized spectral function $\pi\mu_2 a(\lambda)$ at $y = D$ for the conductive case ($\varrho_2/\varrho_1 = 1:10$) and the resistive case ($\varrho_2/\varrho_1 = 10:1$) as function of $\mu_2 D/\pi$. Both figures are dominated by the periodic positive peaks at $\mu_2 = s_n$. In the conductive case the peaks at $\mu_1 = s_n$ impose an additional structure with partly negative peaks, which invalidate a 1-D interpretation. In the resistive case the peaks at $\mu_1 = s_n$ are positive and rapidly fade away with μ_2. For $\mu_2 D/\pi > 6.5$ (not shown) the spectral function attains negative values between successive positive peaks.

The infinite resistivity contrast associated with a perfectly conducting or insulating substratum destroys the 1-D character of the B-response. In general, however, this violation is not serious, as may be anticipated from the small width of the negative peaks or the oscillatory behaviour of the spectral function. As an illustration Fig. 5 of Groom & Bailey (1989) may also serve showing a successful 1-D

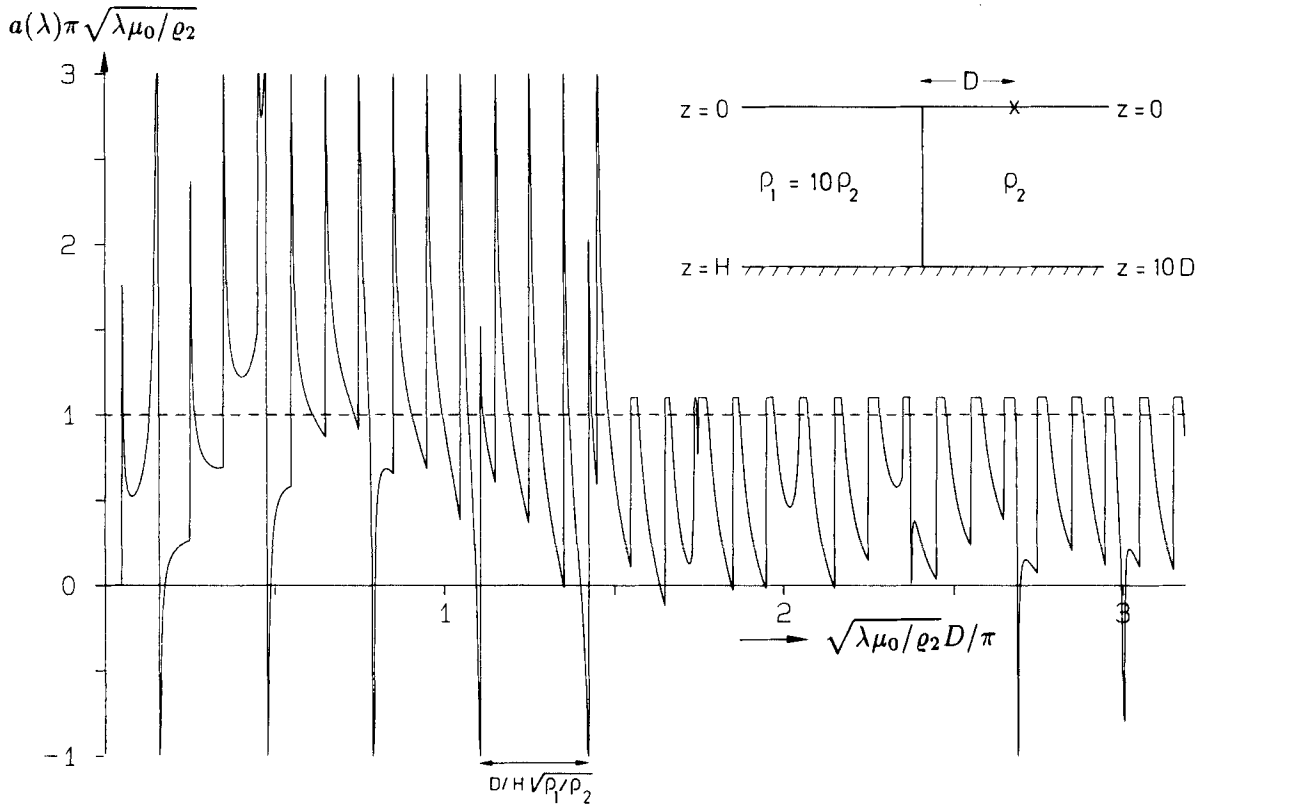

Figure 6. The normalized spectral function at site $y = D$ on a conducting quarter-space ($\varrho_1/\varrho_2 = 10$). The quarter-spaces lie over a perfectly conducting basement at depth $H = 10D$. The spectral function gets its structure by the superposition of two periodic sequences showing in the variable $\mu_2 D/\pi$ the periods D/H and $D/H\sqrt{\varrho_1/\varrho_2}$. The peaks of the latter are mostly negative. For $\mu_2 D/\pi > 1.5$ the positive amplitudes have been truncated.

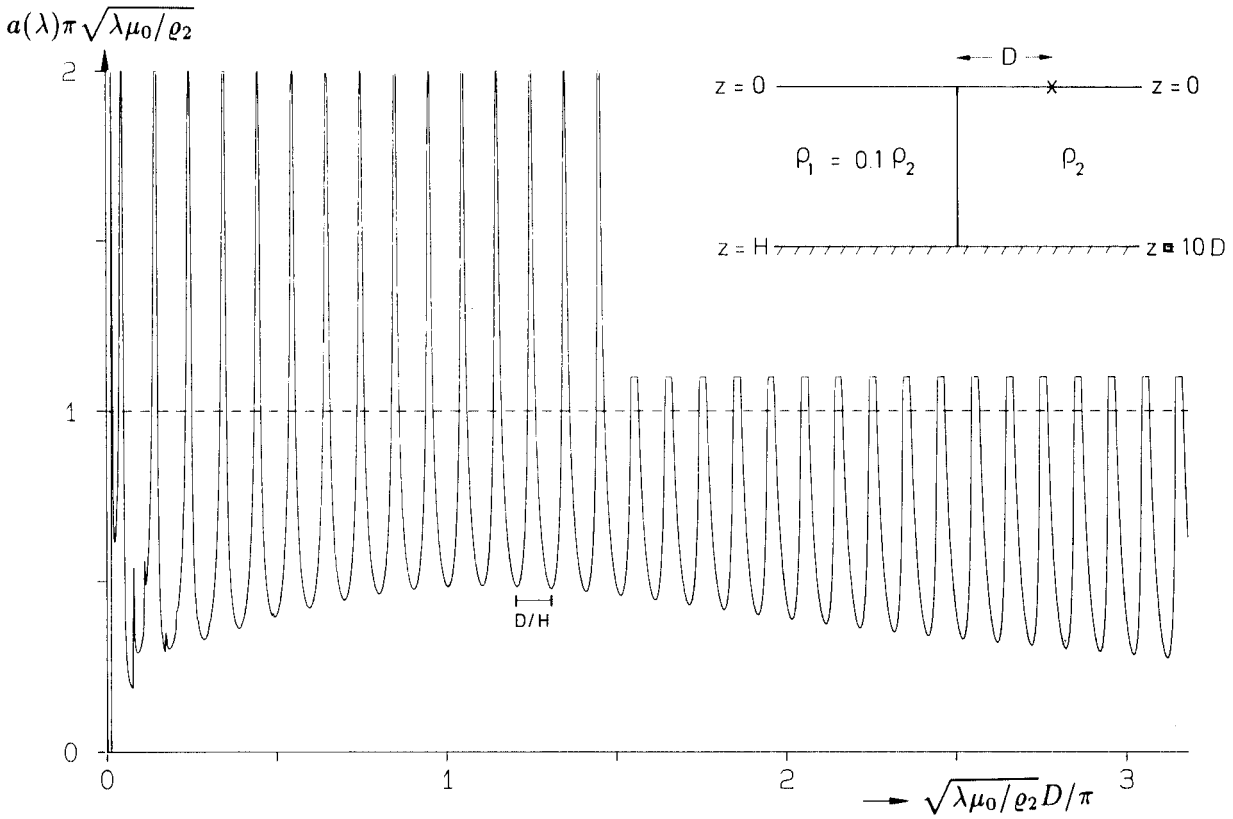

Figure 7. The same as Fig. 6, but on a resistive quarter-space ($\varrho_1/\varrho_2 = 0.1$). Although this is also a superposition of two periodic sequences, the short-period component (period $D/H\sqrt{\varrho_1/\varrho_2}$) is rapidly fading with increasing μ_2. Truncated amplitudes for $\mu_2 D/\pi > 1.5$.

interpretation over a conductive segment of a segmented overburden lying over a resistive basement, albeit the data are not strictly 1-D.

6 RESULTS FROM NUMERICAL MODELLING

The analytical models considered so far have permitted, via the spectral function, a strict test, of whether the B-responses, arbitrarily densely sampled over any frequency interval, admit a 1-D interpretation. In practice, the response is given for a finite set of frequencies. In this case the 1-D test can be performed by means of the necessary and sufficient compatibility conditions as given by Weidelt (1986) or Yee & Paulson (1988b). Even if 1-D interpretability is possible for the given data set, it may be destroyed by increasing the sampling density or shifting the frequency interval.

For an outcropping conducting square-cylinder the B-response in terms of apparent resistivity ϱ_a and phase φ has been computed at the centre of the structure for five frequencies. Along with the response in E-polarization the results are displayed at the top of Fig. 8. The five B-responses successfully pass the 1-D test, whereas the E-responses fail. The B-responses can be represented in terms of D^+-models (Parker 1980). For exact data D^+-models in general are non-unique. The bottom of Fig. 8 shows the two extremal models (Weidelt 1985; Yee & Paulson 1988b): on the left the model

$$c(\omega_j) = \sum_{m=1}^{5} \frac{a_m}{\lambda_m + i\omega_j}, \qquad j = 1, \ldots, 5,$$

which has the shallowest perfect conductor and the greatest surface conductance, and on the right the model

$$c(\omega_j) = \tilde{a}_0 + \sum_{m=1}^{4} \frac{\tilde{a}_m}{\tilde{\lambda}_m + i\omega_j} + \frac{\tilde{a}_5}{i\omega_j}, \quad j = 1, \ldots, 5,$$

showing the least total conductance and the deepest first conductor. By increasing the number of frequencies the extremal models get more and more similar.

This example underlines the well-known fact that the 1-D B-response interpretation may grossly deviate from the true structure, since poor conductors are replaced by fictitious good conductors.

7 A NECESSARY CONDITION FOR B-RESPONSE DATA

According to the eigenfunction expansion given in Appendix A (*cf.* eq. A4) the singularities of the B-response lie on the positive imaginary frequency axis. The angular separation of these singularities from the real frequency axis introduces a particularly smooth frequency dependence. By the transformation $\zeta = \ln \omega$ the ω-plane cut along the positive imaginary axis is mapped on to the fundamental

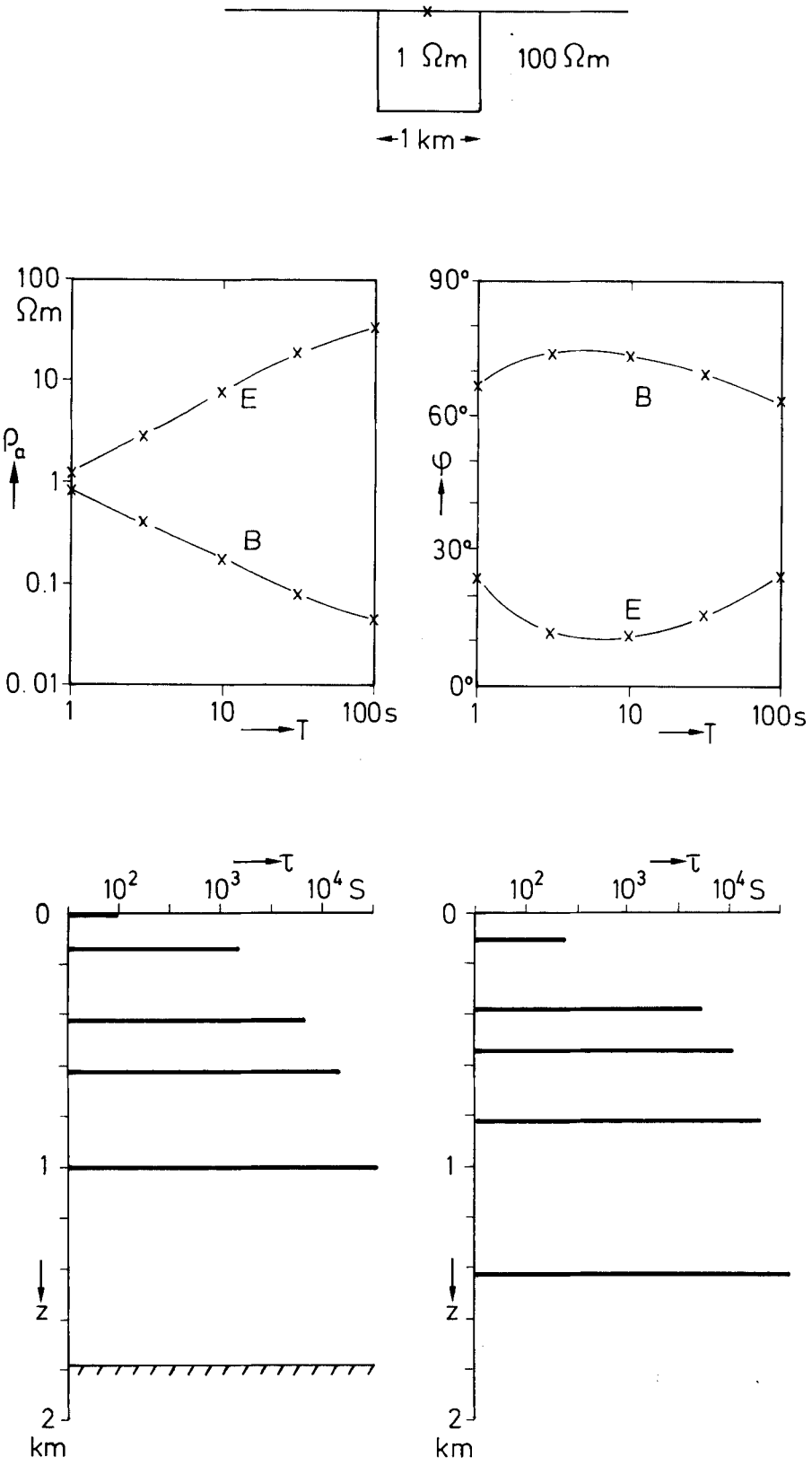

Figure 8. Numerical B- and E-polarization results for a conducting square-cylinder in a resistive host (resistivity contrast 100). Contrary to the E-polarization, the five B-responses satisfy the 1-D constraints. Two of the possible D^+-models explaining the B-response are displayed at the bottom and show false highly conducting layers.

strip $-3\pi/2 < \mathcal{I}\zeta < \pi/2$, which is periodically repeated above and below. The singularities lie along the lines $\mathcal{I}\zeta = (2n + 1/2)\pi$, $n = 0, \pm 1, \pm 2, \ldots$ As an example consider the Mittag–Leffler expansion

$$\frac{1}{1+i\omega} = \frac{1}{1+i\exp(\zeta)} = \frac{1}{2} - \lim_{N\to\infty} \sum_{n=-N}^{+N} \frac{1}{\zeta - (2n+1/2)\pi i}.$$

The data constraints are formulated in terms of the Mellin transform of $c(\omega)$, which corresponds to the Fourier transform in the ζ-domain. If

$$c(\omega) = \begin{cases} O(\omega^{-a}) & \text{for } \omega \to 0 \\ O(\omega^{-b}) & \text{for } \omega \to \infty \end{cases}$$

and $a < b$, then the Mellin transform

$$M(s) = \int_0^\infty c(\omega)\omega^{s-1}\,d\omega = \int_{-\infty}^{+\infty} \bar{c}(\zeta)\exp(\zeta s)\,d\zeta, \qquad s = \sigma + i\tau$$

with $\bar{c}(\zeta) = c(\omega)$ exists for $a < \sigma < b$ (Titchmarsh 1967). For $\tau > 0$ the line of integration in the ζ-plane can be shifted from the real axis to $\mathcal{I}\zeta = \pi/2 - 0$, and for $\tau < 0$ from the real axis to $\mathcal{I}\zeta = -3\pi/2 + 0$ without changing the value of the integral. The evaluation of the resulting integrals then shows that (Titchmarsh 1967)

$$M(s) = \begin{cases} O\left[\exp\left(-\frac{\pi}{2}\tau\right)\right], & \tau \to +\infty \\ O\left[\exp\left(-\frac{3\pi}{2}|\tau|\right)\right], & \tau \to -\infty. \end{cases} \tag{28}$$

A decay $\sim \exp(-\pi|\tau|/2)$ of the Mellin spectrum could easily be inferred from the fact that the closest sources have a distance $h = \pi/2$ from the real axis as line of observation, which in accordance with an elementary theorem in potential theory leads to an $\exp(-h|\tau|)$ decay of the Fourier transform of $\bar{c}(\zeta)$. This decay is in fact observed, if the Fourier transforms of $\mathcal{R}\bar{c}(\zeta)$ and $\mathcal{I}\bar{c}(\zeta)$ are considered separately. However, it is the balance between the real and imaginary parts of an analytical function, which by partial cancellation leads to the sharper decay for $\tau \to -\infty$. Consider for illustration

$$\int_0^\infty \mathcal{R}\left(\frac{1}{1+i\omega}\right)\omega^{s-1}\,d\omega = +\frac{\pi}{2\sin(\pi s/2)},$$

$$\int_0^\infty \mathcal{I}\left(\frac{1}{1+i\omega}\right)\omega^{s-1}\,d\omega = -\frac{\pi}{2\cos(\pi s/2)},$$

$$\int_0^\infty \frac{1}{1+i\omega}\,\omega^{s-1}\,d\omega = \frac{\pi\exp(-i\pi s/2)}{\sin \pi s}$$

with $0 < \sigma < 1$.

It is no easy task to check the asymptotic behaviour (eq. 28) of the Mellin spectrum for real data. The computation requires a broad frequency range and it is not granted that the unbiased extrapolation of the data to $\omega \to 0$ and $\omega \to \infty$ will lead to a B-response $c(\omega)$, for which a Mellin transform

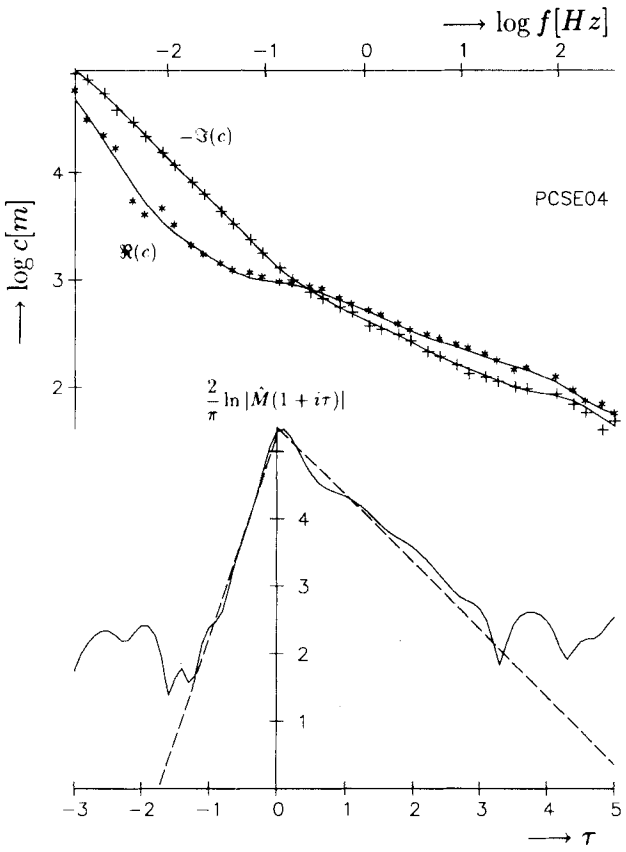

Figure 9. Testing the frequency dependence of B-responses. The top shows real (*) and imaginary parts (+) at the site PCSE04 of the COPROD2 data set. The corresponding logarithmic modified Mellin spectrum is shown at the bottom along with two dashed lines having the postulated asymptotic slope. The Mellin spectrum truncated at $\tau = -1$ and $\tau = 3$ is inverted to yield a smoothed version of the B-response, which is displayed at the top in full lines. It interpolates the real data where they are scattered.

$M(s)$ exists. The COPROD2 data set made available by Dr A. G. Jones provides at 35 sites excellent broad-band B-polarization data over about five to six decades. As an example the top of Fig. 9 shows the B-response at site PCSE04. An extrapolation of the data by assuming $c(\omega) \simeq A(i\omega)^{-a}$ for $\omega \to 0$ and $c(\omega) \simeq B(i\omega)^{-b}$ for $\omega \to \infty$, where a, A, b, and B are real, gives $a = 0.77$ and $b = 0.42$. (The expected value would be $b = 0.5$.) Since $a > b$, no Mellin transform exists for the original data set. As a remedy we replace $c(\omega)$ by

$$\hat{c}(\omega) := \frac{c(\omega)}{1 + i\omega/\omega_0},$$

where $\omega_0 > 0$ is a reference frequency, for which we have chosen the geometric mean of the lowest and highest frequency in the data set. The asymptotic behaviour of $\hat{c}(\omega)$ is characterized by $\hat{a} \simeq a$, $\hat{b} \simeq b + 1$, such that $\hat{c}(\omega)$ has a Mellin transform $\hat{M}(s)$ for $0.77 < \sigma < 1.42$. In theory the modified response $\hat{c}(\omega)$ should also be analytical in $-3\pi/2 < \arg\omega < +\pi/2$ and should satisfy the asymptotic behaviour (eq. 28). Taking $\sigma = 1$, the bottom of Fig. 9 shows the logarithmic Mellin spectrum $(2/\pi)\ln|\hat{M}(1 + i\tau)|$

of the data displayed in the upper part the figure. In this representation we expect the slope +3 for $\tau \to -\infty$ and −1 for $\tau \to +\infty$, which is indicated by the dashed lines and well followed by the experimental data in the range $-1 < \tau < 3$. If the Mellin spectrum is truncated at these bounds and inverted, then

$$\langle c(\omega) \rangle := \frac{1 + i\omega/\omega_0}{2\pi i} \int_{1-i}^{1+3i} \hat{M}(s) \omega^{-s}\, ds$$

is a smoothed version of the data $c(\omega)$ and results from singularities on the positive imaginary ω-axis only. This smoothed version is displayed at the top of Fig. 9 in full lines. The smoothed version differs only slightly from the data and interpolates between them, where they are scattered.

The constraints (eq. 28) of course also hold for true 1-D data, which form a subset of B-polarization data.

8 CONCLUSIONS

The analysis of the magnetotelluric B-polarization response for simple structures has revealed that these data are not fundamentally different from the response of layered conductors. For instance, data from quarter-spaces and dyke models of moderate contrast allow an exact 1-D interpretation. As a practical consequence an excellent 1-D fit to one polarization does not necessarily imply a 1-D structure. However, since in general the data for both polarizations are available, the true dimensionality of the conductor will mostly be uncovered.

On the other hand, the analytical models producing negative peaks in the spectral function (e.g. the highly conducting dyke or the quarter-spaces overlying a perfectly insulating or conducting basement) clearly indicate that in some cases exact B-responses admit only an approximate 1-D interpretation. Because of the deficiencies of real data, it will in practice mostly be impossible to attribute a 1-D misfit—without considering the second polarization—either to data errors or to a 1-D inconsistency (*cf.* Fig. 5 of Groom & Bailey (1989)).

B-response and 1-D response are closely related, because both admit the representation (4) or (6), i.e. the singularities are located on the positive imaginary frequency axis, which considerably constrains the frequency dependence as illustrated in Section 7. Such a presentation is not granted for the E-polarization response, which is the ratio of two disturbed field components. Moreover—and this is not a consequence of eq. (4)—the phases of B-response and 1-D response are restricted to the same quadrant. The difference between the responses results from the incidental negative values of the spectral function $a(y, \lambda)$. In the examples studied, the negative peaks were either narrow or the spectral function was highly oscillatory between (great) positive and (small) negative values, so that in a real data set this 1-D inconsistency may be hidden.

ACKNOWLEDGMENTS

To Dr Alan Jones we convey our sincere thanks for providing the COPROD2 data set. P.K. gratefully acknowledges the support by the Alexander von Humboldt Foundation. Dr Colin Farquharson and an unknown referee have contributed valuable suggestions for improving the manuscript.

REFERENCES

Berdicevskij, M.N. & Dmitriev, V.I., 1992. *Magnetotelluric Soundings of Horizontally Uniform Media*, Nedra, Moscow (in Russian).

d'Erceville, I. & Kunetz, G., 1962. The effect of a fault on the Earth's natural electromagnetic field, *Geophysics*, **27**, 651–665.

Fischer, G. & Schnegg, P.-A., 1980. The dispersion relations of the magnetotelluric response and their incidence on the inversion problem, *Geophys. J.R. astr. Soc.*, **62**, 661–673.

Groom, R.W. & Bailey, R.C., 1989. Some effects of multiple lateral inhomogeneities in magnetotellurics, *Geophys. Prosp.*, **37**, 697–712.

Nussenzveig, H.M., 1972. *Causality and Dispersion Relations*, Academic Press, New York.

Parker, R.L., 1980. The inverse problem of geomagnetic induction: existence and construction of solutions based on incomplete data, *J. geophys. Res.*, **85**, 4421–4428.

Protter, M.. & Weinberger, H.F., 1967. *Maximum Principles in Differential Equations*, Prentice-Hall, Englewood Cliffs, NJ.

Rankin, D., 1962. The magnetotelluric effect on a dike, *Geophysics*, **27**, 666–676.

Schmucker, U., 1970. Anomalies of geomagnetic variations in the southwestern United States, *Bull. Scripps. Inst. Ocean. Univ. Calif.*, **13**, 1–165.

Titchmarsh, E.C., 1967. *Introduction to the theory of Fourier integrals*, 2nd edn, Oxford University Press, London.

Wait, J.R. & Spies, K.P., 1974. Magneto-telluric fields for a segmented overburden, *J. Geomagn. Geoelect.*, **26**, 449–458.

Weidelt, P., 1972. The inverse problem of geomagnetic induction, *Z Geophys.*, **38**, 257–289.

Weidelt, P., 1985. Construction of conductance bounds from magnetotelluric impedances, *J. Geophys.*, **57**, 191–206.

Weidelt, P., 1986. Discrete frequency inequalities for magnetotelluric impedances of one-dimensional conductors, *J. Geophys.*, **59**, 171–176.

Whittall, K.P. & Oldenburg, D.W., 1986. Inversion of magnetotelluric data using a practical inverse scattering formulation, *Geophysics*, **51**, 383–395.

Yee, E. & Paulson, K.V., 1988a. Properties of the c-response function for conductivity distributions of class S^+, *Geophys. J.*, **93**, 265–278.

Yee, E. & Paulson, K.V., 1988b. Necessary and sufficient conditions for the existence of a solution to the one-dimensional magnetotelluric inverse problem, *Geophys. J.*, **93**, 279–293.

APPENDIX A: EIGENFUNCTION REPRESENTATION OF THE B-RESPONSE

The electromagnetic field in the half-space $z \geq 0$ can be represented by a superposition of the magnetic field free-decay modes

$$B_n(y, z, t) = f_n(y, z) \exp(-\lambda_n t),$$

where $\lambda_n \geq 0$ is the decay constant. Even though the decay spectrum becomes continuous for unbounded conductors, for ease of notation all possible quantum numbers are symbolically represented by the discrete quantum number n.

The modes $f_n(y, z)$ are defined as eigenfunctions of the problem

$$\nabla \cdot (\varrho \nabla f_n) + \lambda_n \mu_0 f_n = 0, \qquad z \geq 0, \qquad f_n(y, 0) = 0 \qquad \text{(A1)}$$

with $\lambda_n \geq 0$ as eigenvalue. They are orthogonal, normalized by

$$\int_{z\geq 0} f_n(y, z) f_{n'}^*(y, z)\, dy\, dz = \delta_{nn'}, \tag{A2}$$

where $\delta_{nn'}$ is the Kronecker symbol, and form a complete set of functions. Therefore $\beta := B_x/B_0$ admits the representation

$$\beta(y, z, \omega) = \sum_n \alpha_n(\omega) f_n(y, z), \tag{A3}$$

where by virtue of eq. (A2)

$$\alpha_n(\omega) = \int_{z\geq 0} \beta(y, z, \omega) f_n^*(y, z)\, dy\, dz.$$

The expansion coefficient α_n is obtained by multiplying the complex conjugate of eq. (A1) by β, eq. (1) (formulated in terms of β) by f_n^* and integrating the difference over the half-space $z \geq 0$. Integration by parts on using the boundary values $f_n(y, 0) = 0$, $\beta(y, 0, \omega) = 1$ yields

$$\alpha_n(\omega) = \frac{1}{\lambda_n + i\omega} \int_{-\infty}^{+\infty} g_n^*(\eta)\, d\eta$$

with

$$g_n(y) := \frac{\varrho(y, 0)}{\mu_0} \partial_z f_n(y, z)|_{z=0}.$$

The boundary values of f_n and β imply that eq. (A3) is non-uniformly convergent at $z = 0$. Therefore eq. (A3) cannot be differentiated with respect to z to obtain according to (eq. 3) the B-response $c(y, \omega)$. As a remedy it is noted that no induction occurs at $\omega = 0$, and therefore

$$1 = \beta(y, z, 0) = \sum_n \alpha_n(0) f_n(y, z)$$

and

$$\beta(y, z, \omega) = 1 + \sum_n [\alpha_n(\omega) - \alpha_n(0)] f_n(y, z).$$

The latter version converges uniformly at $z = 0$ and forms the basis for the construction of $c(y, \omega)$ from eq. (3),

$$c(y, \omega) = \sum_n \frac{a_n(y)}{\lambda_n + i\omega} \tag{A4}$$

with

$$a_n(y) := \frac{1}{\lambda_n} g_n(y) \int_{-\infty}^{+\infty} g_n^*(\eta)\, d\eta. \tag{A5}$$

The spectral function $a(y, \lambda)$ is obtained by summing all $a_n(y)$ with $\lambda_n = \lambda$. Since in general eigenfunctions are oscillating, individual $a_n(y)$ will have both signs. However, the summation of expansion coefficients belonging to the same eigenvalue may give a positive yield, which is necessary for a 1-D interpretation. This is illustrated by the quarter-space model considered below. Moreover, expansion coefficients $a_n(y)$ sufficiently averaged over y will tend to positive values, since according to eq. (A5) a_n then will approach the product of two complex conjugate numbers.

The B-response eigenfunction expansion (A4) is illustrated by two simple examples.

1 Uniform half-space of resistivity ϱ in $z \geq 0$

The discrete quantum number n is replaced by the two continuous quantum numbers u and v. The eigenfunctions

$$f_{uv}(y, z) = \frac{1}{\pi} \exp(iuy) \sin(vz), \quad -\infty < u < +\infty, \quad 0 \leq v < \infty$$

with the eigenvalues

$$\lambda_{uv} = \varrho(u^2 + v^2)/\mu_0$$

are normalized by

$$\int_{z\geq 0} f_{uv}(y, z) f_{u'v'}^*(y, z)\, dy\, dz = \delta(u - u')\delta(v - v'). \tag{A6}$$

With

$$a_{uv} = \frac{2\varrho}{\mu_0 \pi} \frac{v^2}{u^2 + v^2} \exp(iuy)\delta(u) = \frac{2\varrho}{\mu_0 \pi} \delta(u)$$

the 'B-response' is given by

$$c(\omega) = \int_{-\infty}^{+\infty} du \int_0^{\infty} dv \frac{a_{uv}}{\lambda_{uv} + i\omega}$$
$$= \frac{2}{\pi} \int_0^{\infty} \frac{dv}{v^2 + i\omega\mu_0/\varrho} = \sqrt{\frac{\varrho}{i\omega\mu_0}}.$$

Because of the lateral uniformity there is a contribution only from the horizontal wavenumber $u = 0$.

2. Two quarter-spaces with resistivity ϱ_1 in $y < 0$ and ϱ_2 in $y > 0$

This model is considered in Section 3. Let again $r := \varrho_2/\varrho_1$. Without restricting generality we assume $\varrho_2 < \varrho_1$ such that $r < 1$. Since in the vertical direction the quarter-spaces extend to infinity, the ansatz

$$f(y, z) = \varphi(y) \sin(vz) \tag{A7}$$

is appropriate. From eq. (A1) follows

$$\varphi''(y) + (\mu_m^2 - v^2)\varphi(y) = 0, \quad \mu_m^2 := \lambda\mu_0/\varrho_m, \tag{A8}$$

with $m = 1$ for $y < 0$ and $m = 2$ for $y > 0$, and $\mu_1 < \mu_2$. Eq. (A8) is supplemented by requiring the continuity of φ and $\varrho\varphi'$ at $y = 0$. The resulting eigenfunctions are always oscillatory in the well-conducting quarter-space $y > 0$. In $y < 0$, however, they are oscillating only for $v < \mu_1$ and exponentially damped for $v > \mu_1$.

(a) $0 < v < \mu_1 < \mu_2$

The eigenfunctions oscillate with the vertical wavenumber v and the horizontal wavenumbers $u_m = \sqrt{\mu_m^2 - v^2}$, which according to the definition of μ_m are interrelated by

$$u_1^2 = ru_2^2 - (1 - r)v^2. \tag{A9}$$

Therefore the two quantum numbers u_2 and v are sufficient to characterize the eigenfunctions and corresponding eigenvalues. The latter are

$$\lambda_{u_2 v} = \varrho_1(u_1^2 + v^2)/\mu_0 = \varrho_2(u_2^2 + v^2)/\mu_0. \tag{A10}$$

There are two sets of eigenfunctions, which in the limit $r \to 1$ are anti-symmetrical or symmetrical to the origin.

Normalized as eq. (A6) (with u replaced by u_2) they read

$$f^{(1)}_{u_2 v}(y, z) = \frac{2 \sin(vz)}{\pi \sqrt{u_1(u_1 + r u_2)}} \begin{cases} r u_2 \sin(u_1 y), & y < 0 \\ u_1 \sin(u_2 y), & y > 0 \end{cases}$$

$$f^{(2)}_{u_2 v}(y, z) = \frac{2\sqrt{r u_2} \sin(vz)}{\pi \sqrt{u_1 + r u_2}} \begin{cases} \cos(u_1 y), & y < 0 \\ \cos(u_2 y), & y > 0 \end{cases}$$

with $0 \le u_2 < \infty$, $0 \le 0 \le \sqrt{r/(1-r)}\, u_2$. The latter limit follows from eq. (A9) for $u_1 \to 0$. A closer examination shows that only the first set contributes to the spectral function. The expansion coefficient corresponding to eq. (A5) is

$$a^{(1)}_{u_2 v}(y) = -\frac{2\gamma(1-r)v^2}{\pi^2 u_1 u_2 (u_1 + r u_2)} \begin{cases} \sin(u_1 y)/u_1, & y < 0 \\ \sin(u_2 y)/u_2, & y > 0 \end{cases} \tag{A11}$$

with $\gamma := 2\varrho_2 u_2/\mu_0$. The reason for introducing this factor will become apparent below.

(b) $\mu_1 < v < \mu_2$

Now the wavenumber u_1 is purely imaginary and the eigenfunctions in $y < 0$ are exponentially damped. Let $\bar{u}_1 := \sqrt{v^2 - \mu_1^2} > 0$ where $\bar{u}_1$ is related to u_2 and v by

$$\bar{u}_1^2 = (1-r)v^2 - r u_2^2. \tag{A12}$$

The eigenvalues and normalized eigenfunctions are

$$\lambda_{u_2 v} = \varrho_1(v^2 - \bar{u}_1^2)/\mu_0 = \varrho_2(u_2^2 + v^2)/\mu_0 \tag{A13}$$

$$f^{(3)}_{u_2 v} = \frac{2 u_2 \sin(vz)}{\pi \sqrt{\bar{u}_1^2 + r^2 u_2^2}} \times \begin{cases} r \exp(\bar{u}_1 y), & y < 0 \\ [r \cos(u_2 y) + \bar{u}_1 \sin(u_2 y)/u_2], & y > 0 \end{cases} \tag{A14}$$

with $0 \le u_2 < \infty$, $v > \sqrt{r/(1-r)}\, u_2$. The latter limit refers to $\bar{u}_1 \to 0$ (*cf.* eq. A12). Eq. (A5) provides as B-response expansion coefficient

$$a^{(3)}_{u_2 v}(y) = \frac{2\gamma v^2}{\pi^2 \bar{u}_1 u_2 (\bar{u}_1^2 + r v^2)} \times \begin{cases} \exp(\bar{u}_1 y), & y < 0 \\ [r \cos(u_2 y) + \bar{u}_1 \sin(u_2 y)/u_2], & y > 0. \end{cases} \tag{A15}$$

Now we are in the position to synthesize $c(y, \omega)$. From eqs (A4) and (4) follows

$$c(y, \omega) = \int_0^\infty du_2 \int_0^\infty \frac{a_{u_2 v}(y)\, dv}{\lambda_{u_2 v} + i\omega} = \int_0^\infty \frac{a(y, \lambda)\, d\lambda}{\lambda + i\omega}. \tag{A16}$$

In the first version the integration over the first quadrant of the (u_2, v)-plane is performed along axis-parallel strips, in the second version along circular arcs of radius $\sqrt{u_2^2 + v^2} = \mu_2$, where $\lambda_{u_2 v}$ is constant, $\lambda_{u_2 v} = \lambda$ (*cf.* eqs A10 and A8). If the pair (u_2, v) is replaced by (λ, v), eq. (A10) gives $d\lambda = \gamma\, du_2$, and therefore the expansion coefficients $a_{u_2 v}(y)$ are related to the spectral function $a(y, \lambda)$ by

$$a(y, \lambda) = \int_0^{\mu_2} a_{u_2 v}(y)/\gamma\, dv,$$

the pair (u_2, v) is replaced by (λ, v), eq. (A10) gives $d\lambda = \gamma\, du_2$, and therefore the expansion coefficients $a_{u_2 v}(y)$ are related to the spectral function $a(y, \lambda)$ by

$$a(y, \lambda) = \int_0^{\mu_2} a_{u_2 v}(y)/\gamma\, dv,$$

where u_1, $\bar{u}_1$, and u_2 have to be expressed via eqs (A10) and (A13) by λ and v. From eqs (A11) and (A15) follows for instance for $y > 0$

$$\pi a(y, \lambda) = -\frac{2(1-r)}{\pi} \int_0^{\mu_1} \frac{v^2 \sin(u_2 y)\, dv}{u_1 u_2^2 (u_1 + r u_2)} + \frac{2}{\pi} \int_{\mu_1}^{\mu_2} \frac{u^2 [r \cos(u_2 y) + \bar{u}_1 \sin(u_2 y)/u_2]\, dv}{\bar{u}_1 u_2 (\bar{u}_1^2 + r v^2)}. \tag{A17}$$

A corresponding expression is obtained for $y < 0$. These expressions are formally more complicated than eq. (16), and their positivity is not easily established, but they agree exactly with the results obtained by applying the recipe (5) to eqs (13) and (14). The correspondences are $s \to v$, $k_m^2 \to -\mu_m^2$, $\alpha_1 \to i u_1$ or $\bar{u}_1$, $\alpha_2 \to i u_2$. The terms α_m^2 in the denominators of eqs (13) and (14) lead to poles at $s = \mu_m$, which cancel the contributions from the first term $1/k_m$. For $r \to 1$ the second integral of eq. (A17) yields a non-vanishing contribution, since in this case $\bar{u}_1 \simeq u_2 \simeq 0$, $\mu_1 \simeq \mu_2 \simeq v$ and (for all $r < 1$)

$$\frac{2}{\pi} \int_{\mu_1}^{\mu_2} \frac{v\, dv}{\bar{u}_1 u_2} = 1.$$

The B-response is obtained from the first version of eq. (A16) after changing the order of integration, since the v-integration in eq. (A16) corresponds to the s-integration in eqs (13) and (14).

APPENDIX B: THE B-RESPONSE OF A SEGMENTED HALF-SPACE

In this appendix we describe a new method for calculating the B-response of a segmented half-space and show that its 1-D interpretation gives the correct resistivity down to the depth of half the distance to the closest interface.

Considered is the simple resistivity model $\varrho(y, z) = \varrho(y)/\Theta(z)$, where $\Theta(z)$ is the Heaviside function. Let the Green function $G_s(y \mid \eta)$ with $G_s(\pm\infty \mid \eta) = 0$ be the solution of

$$\partial_y[\varrho(y)\partial_y G_s(y \mid \eta)] = \varrho(y)\alpha^2(y) G_s(y \mid \eta) - \delta(y - \eta), \tag{B1}$$

where $\alpha^2(y) := s^2 + i\omega\mu_0/\varrho(y)$. Then it is easily verified that

$$B_x(y, z)/B_0 = 1 - \frac{2i\omega\mu_0}{\pi} \int_0^\infty ds\, \frac{\sin(sz)}{s} \int_{-\infty}^{+\infty} G_s(y \mid \eta)\, d\eta$$

satisfies eq. (1) with the boundary condition eq. (2). Therefore, according to eq. (3)

$$c(y) = \frac{2\varrho(y)}{\pi} \int_0^\infty ds \int_{-\infty}^{+\infty} G_s(y \mid \eta)\, d\eta. \tag{B2}$$

For an N-segmented half-space

$$\varrho = \varrho_n \quad \text{in} \quad y_{n-1} < y < y_n,$$

where

$$n \in [1, N], \qquad y_0 = -\infty, \qquad y_N = +\infty$$

the η-integration in eq. (B2) can be replaced by a sum over the $N-1$ resistivity discontinuities. For this purpose we interchange in eq. (B1) the variables y and η and solve for $G_s(\eta \mid y)$, which is inserted in eq. (B2) on noting the reciprocity $G_s(y \mid \eta) = G_s(\eta \mid y)$. Then integration by parts yields

$$\begin{aligned} c(y) &= \frac{1}{k(y)} - \frac{2\varrho(y)}{\pi} \int_0^\infty ds \\ &\quad \times \int_{-\infty}^{+\infty} \varrho(\eta) \partial_\eta G_s(\eta \mid y) \partial_\eta [\varrho(\eta)\alpha^2(\eta)]^{-1} \, d\eta \\ &= \frac{1}{k(y)} - \frac{2\varrho(y)}{\pi} \sum_{n=1}^{N-1} \frac{\varrho_n - \varrho_{n+1}}{\varrho_n \varrho_{n+1}} \\ &\quad \times \int_0^\infty [\varrho(\eta)\partial_n G_s(\eta \mid y)]_{\eta = y_n} \frac{s^2 \, ds}{\alpha_n^2 \alpha_{n+1}^2} \end{aligned} \tag{B3}$$

with $k^2(y) := i\omega\mu_0/\varrho(y)$ and $\alpha_n^2 := i\omega\mu_0/\varrho_n$. Since $c(y)$ is discontinuous at $y = y_n$, we assume in the sequel that y does not coincide with an interface. For ease of presentation we introduce instead an artificial interface with no resistivity contrast at $\eta = y$ (and increase N by 1). Let $y = y_m$. Then

$$g_n := [\varrho(\eta)\partial_\eta G_s(\eta \mid y_m)]_{\eta = y_n}$$

is continuous at interfaces and is easily obtained by recursion. Let $d_n := y_n - y_{n-1}$, $n = 2, \ldots, N-1$ be the thicknesses of the interior segments and let $t_n := \tanh(\alpha_n d_n)$, $\gamma_n := \alpha_n \varrho_n$. Then the transfer functions $b_n^- := +g_n / G_s(y_n \mid y_m)$ of the field diffusing from the source point y_m into $y \to -\infty$ are obtained from

$$b_n^- = \gamma_n \frac{b_{n-1}^- + \gamma_n t_n}{\gamma_n + b_{n-1}^- t_n}, \qquad n = 2, \ldots, m, \tag{B4}$$

where $b_1^- = \gamma_1$. The corresponding transfer functions for a diffusion into $y \to +\infty$, $b_n^+ := -g_n / G_s(y_n \mid y_m)$, are

$$b_{n-1}^+ = \gamma_n \frac{b_n^+ + \gamma_n t_n}{\gamma_n + b_n^+ t_n}, \qquad n = N-1, \ldots, m+1,$$

where $b_{N-1}^+ = \gamma_N$. The presence of the source point at y_m introduces a discontinuity in the slope of $G_s(\eta \mid y_m)$, such that according to eq. (B1) $g_m^+ - g_m^- = -1$. Together with $b_m^- = g_m^- / G_s(y_m \mid y_m)$ and $b_m^+ = -g_m^+ / G_s(y_m \mid y_m)$ this yields

$$G_s(y_m \mid y_m) = \frac{1}{b_m^- + b_m^+}, \quad g_m^- = +\frac{b_m^-}{b_m^- + b_m^+}, \quad g_m^+ = -\frac{b_m^+}{b_m^- + b_m^+}.$$

For the field diffusing into $y \to -\infty$ one easily obtains

$$g_{n-1} = g_n [\cosh(\alpha_n d_n) - (\gamma_n / b_n^-) \sinh(\alpha_n d_n)], \quad n = m, \ldots, 2.$$

Expressing the hyperbolic functions by exponentials and replacing positive exponents by negative exponents on using the symmetrical relation

$$\frac{b_{n-1}^- + \gamma_n}{b_n^- + \gamma_n} \exp(+\alpha_n d_n) = \frac{b_{n-1}^- - \gamma_n}{b_n^- - \gamma_n} \exp(-\alpha_n d_n),$$

following from eq. (B4), we finally arrive at

$$g_{n-1} = g_n \frac{1 + \gamma_n / b_n^-}{1 + \gamma_n / b_{n-1}^-} \exp(-\alpha_n d_n), \qquad n = m, \ldots, 2, \tag{B5}$$

starting with $g_m = g_m^-$. A similar treatment for $n > m$ yields the recursion

$$g_n = g_{n-1} \frac{1 + \gamma_n / b_{n-1}^+}{1 + \gamma_n / b_n^+} \exp(-\alpha_n d_n), \qquad n = m+1, \ldots, N-1, \tag{B6}$$

starting with $g_m = g_m^+$. Because of the vanishing resistivity contrast ($\varrho_m = \varrho_{m+1}$), the discontinuous term g_m^+ does not contribute to the sum in eq. (B3).

The similar problem of a segmented overburden overlying a perfectly conducting or insulating basement is treated by restricting the vertical wavenumber s to discrete values. The comparison of eq. (14) with eqs (26) or (27) shows the appropriate substitutions. A different method to handle the segmented overburden model was proposed by Wait & Spies (1974).

Now we turn to the 1-D interpretation of the B-response. Let $k := \sqrt{i\omega\mu_0/\varrho(y)}$. Because of the presentation eq. (4) $c(y, \omega)$ is analytical in the ω-plane cut along the positive imaginary axis. This implies that $c(k) := c(y, \omega)$ is analytical in the half-plane $\Re k > 0$. With the definition of Section 3.2, $\mu := \sqrt{\lambda\mu_0/\varrho(y)}$ and $\tilde{a}(\mu) := a(\lambda)$ the presentation eq. (4) yields

$$b(k) := \tfrac{1}{2}[1 - kc(k)] = \frac{k}{\pi} \int_0^\infty \frac{1 - \pi\mu\tilde{a}(\mu)}{\mu^2 + k^2} \, d\mu.$$

Therefore

$$\begin{aligned} &\frac{1}{2\pi i} \int_{\epsilon - i\infty}^{\epsilon + i\infty} b(k) \exp(kx) \, dk \\ &\quad = \frac{1}{\pi} \int_0^\infty [1 - \pi\mu\tilde{a}(\mu)] \cos(\mu x) \, d\mu = B(x), \qquad \epsilon > 0. \end{aligned} \tag{B7}$$

We have arrived at the last result after changing the order of integrations, performing the k-integration by the calculus of residues, and resuming the definition eq. (18) of $B(x)$. Hence, $b(k)$ is the Laplace transform of $B(x)$.

Now the behaviour of $b(k)$ for $|k| \to \infty$ in the right half-plane has to be investigated. In view of the exponential decay displayed in eqs (B5) and (B6), the dominant contribution in the sum eq. (B3) comes from the term $n = m-1$ or $n = m+1$, according to whether the interface y_{m-1} or y_{m+1} is closer to y. Let y_{m-1} be the closer interface and let $D := y - y_{m-1}$. Then

$$b(k) \simeq \frac{k}{\pi} \frac{\varrho_{m-1} - \varrho(y)}{\varrho_{m-1}} \int_0^\infty g_{m-1}(s, k) \frac{s^2 \, ds}{\alpha^2(y)\alpha_{m-1}^2}.$$

Since for $|k| \to \infty$

$$g_{m-1}(s, k) \simeq \frac{\gamma_{m-1}}{\gamma(y) + \gamma_{m-1}} \exp(-kD),$$

$b(k)$ decays at least as fast as $\exp(-kD)$. Hence for $x < D$ the contour in eq. (B7) can be closed by a large semi-circle in the half-plane $\Re k > 0$ without changing the value of the integral. Since $b(k)$ is analytical in its interior, $B(x) = 0$ for $x < D$. The 1-D construction method from Section 3.2 then shows that the correct resistivity $\varrho(y)$ is recovered down to the depth of $D/2$. In the segmented overburden model the resistivity is correct down to the depth $\min(H, D/2)$.